6th European Conference on Computational Mechanics (ECCM 6)
7th European Conference on Computational Fluid Dynamics (ECFD 7)
11 – 15 June 2018, Glasgow, UK

INVESTIGATION OF TEXTURE EVOLUTION DURING ROLLING SIMULATION OF NON-ORIENTED SI BASED ELECTRICAL STEELS WITH 2D AND 3D RVE

A. VUPPALA [1*, a], X. WEI[2,a], S. HOJDA[3,a], M. TELLER[4,a] AND G. HIRT[5,a]

[1*] Corresponding Author: vuppala@ibf.rwth-aachen.de

[2] wei@ibf.rwth-aachen.de

[3]hojda@ibf.rwth-aachen.de

[4] teller@ibf.rwth-aachen.de

[5]hirt@ibf.rwth-aachen.de

[a] RWTH Aachen University. Institute of Metal Forming (IBF)
Intzestr. 10, 52056 Aachen, Germany

Key words: Texture prediction, CPFEM, 3D vs 2D RVE simulations, Flat rolling process, BCC Electrical Steels, DAMASK

Abstract. The process chain of non-oriented silicon based electrical steels consists of continuous casting, hot rolling with considerate heat treatment followed by cold rolling and final heat treatment. Every step in this process chain has an influence on the microstructure development like texture and grain size, which in turn influence the desired electromagnetic properties (low iron losses and good magnetic flux densities). Texture evolution during cold rolling plays a major role on the recrystallization (RX) characteristics (RX texture and grain growth) in the final heat treatment. To optimize the texture evolution in cold rolling in order to obtain better electromagnetic properties a verified simulation model is necessary. For this purpose, hot band strips are cold rolled in three consecutive passes for 50 % height reduction. After each pass macro texture was measured to evaluate the texture evolution. This multi pass rolling process is simulated in a top-down multiscale modelling approach where elasto-plastic based FEM simulations of cold rolling are performed to obtain the history of the deformation gradient at the centre of the workpiece. This history variable is then imposed on a polycrystal Representative Volume Element (RVE) using a phenomenological Crystal Plasticity FEM (CPFEM) material model developed in DAMASK crystal plasticity tool. The influence of the RVE dimension on the predicted texture evolution is analysed by the comparison of a 2D RVE simulation to a 3D RVE simulation. Thereafter, the fibre texture intensities from both models are compared with the experimental results. The 3D RVE is able to predict the experimentally measured texture evolution more precisely and thus overcoming the limitation of a 2D RVE.

1 INTRODUCTION

Non-oriented electrical steel parts are essential components of electrical machines. Improving the performance of electrical machines would improve the overall efficiency of electrical vehicles, and thus contributing to the growing needs of regenerative energy sources in automobile industry. The machinery cores in electrical motors and generators are manufactured from non-oriented electrical steels because the direction of the magnetic flux is not constant in the rotating parts. Each step in the manufacturing process of these components shows a significant impact on the final desired magnetic properties which include low iron losses, high permeability and induction [1,2]. Cold rolling is one of the process steps in production of non-oriented silicon steel components. The general textures observed after cold rolling of these type of BCC steels are the α-fiber (<110> || Rolling Direction (RD)) and γ-fibre (<111> || Normal Direction (ND)) [2]. This texture is influenced by different processing conditions like the rolling method (flat rolling, asymmetric rolling), rolling schedules as well as the microstructural conditions like the initial grain size and final heat treatment processes, in turn these dependencies influence the service properties of the components. Performing multiple rolling experiments is time consuming and expensive. To consider the influence of different parameters and obtain desired magnetic properties, a simulation model would be useful. The model can be used to study the influence of process parameters and input conditions. Texture evolution can be studied with different simulation methods like the Taylor model, Advanced Lamel (ALAMEL) model [3], Visco-Plastic Self-Consistent (VPSC) model [4] and CPFEM [5]. There exists literature where different texture analysis methods have been studied comparatively [6]. These methods were mainly studied to obtain the effective mechanical properties of polycrystals. But the aim of the current project is to obtain as precise texture as possible so that the deformed texture from the RVE can be used in future to simulate the annealing conditions. Though CPFEM is computationally expensive, it is a robust method to obtain accurate texture during the mechanical deformation processes. Phenomenological constitutive model in CPFEM considers the material state only with respect to the critical resolved shear stresses on the slip system. This makes the method simple to use with minimum number of input parameters and is computationally effective.

In this paper, rolling trials are conducted on a 1 *mm* thick sheet for a thickness reduction of 50 % in three passes. Macro texture is measured after each pass with X-Ray diffraction (XRD). Then, the macro scale rolling process is simulated in Abaqus/Standard and the obtained deformation gradient is used as a boundary condition on the representative volume element (RVE) to obtain the texture during the rolling process. The 3D RVE has 300 grains with characteristic initial texture. The phenomenological material model implemented in DAMASK [5] is used in this work. The simulations results are compared with 2D simulations performed in a previous study [7].

2 THEORY

2.1 CPFEM Constitutive Model

The constitutive model used in this paper is implemented in the CPFEM tool box DAMASK [5]. The basis for CPFEM formulation is the plastic velocity gradient equation which relates the shear rate on a slip system α with the slip direction m^{α} and slip plane normal

n^α by

$$\boldsymbol{L_p} = \dot{\gamma}^\alpha \, m^\alpha \otimes n^\alpha. \tag{1}$$

Phenomenological constitutive power law uses the critical resolved shear stress τ_α^c as the material state variable. For this reason, the shear rate $\dot{\gamma}^\alpha$, on a particular slip system α is considered as a function of the critical resolver shear stress and resolved shear stress τ_α as

$$\dot{\gamma}^\alpha = \dot{\gamma}_0 \left|\frac{\tau_\alpha}{\tau_\alpha^c}\right|^n dir(\tau_\alpha) \tag{2}$$

$\dot{\gamma}_0$ is referred to as reference strain rate and *n* is the strain rate sensitivity parameter. $dir(\tau_\alpha)$ determines the direction of the shear rate. These parameters have to be determined by an appropriate fitting procedure that is described later.

The hardening behavior τ_α^c on a slip system α is determined by its influence with other slip system β by the evolution relationship

$$\dot{\tau_\alpha^c} = q_{\alpha\beta} h_0 \left(1 - \frac{\tau_\beta^c}{\tau_\infty}\right)^a |\dot{\gamma}^\beta| \tag{3}$$

where the factor $q_{\alpha\beta}$ is needed to model self $(\alpha = \beta)$ and lateral hardening behavior $(\alpha \neq \beta)$. h_0, a, and τ_∞ are the slip hardening parameters which depend on the material behaviour.

2.2 Experimental Details

The process chain of semi-finished products produced from electrical steel consists of four major steps. The steel is casted as continuous slabs, hot rolled and pre-annealing is performed. These strips are then cold rolled and thereafter heat treated to obtain the desired magnetic properties and also to guarantee formability during the subsequent cutting operations. The strips obtained after hot rolling have a thickness of 1 *mm*. The chemical composition of the hot rolled samples is shown in Table 1.

Table 1: Chemical composition of hot strips

Chemical Element	Si	Al	Mn	P	S	C	Fe
Weight (in %)	2.4	0.39	0.30	0.021	0.003	0.002	balance

The hot strips are cold rolled with three consecutive passes for a total thickness reduction of 50 %. The macro texture is measured before cold rolling and after each pass by XRD with "D8 Advance" from Bruker by our project partner Institute of Physical Metallurgy and Metal Physics (IMM) at RWTH Aachen. The measurements were performed on the center of the strips on a measuring area of 144 mm^2 in the rolling-transverse plane. The initial XRD data is used to obtain the orientations of the grains as Euler angles which are the input for the simulation model.

Additionally, stacked layer compression tests were performed at room temperature at four strain rates 0.01 s^{-1}, 0.1 s^{-1}, 1 s^{-1} and 10 s^{-1} to obtain the flow curves. The height reduction in the stacked layer samples is only from 15 *mm* to 13 *mm* and thus the final strain in the

experimental results is approximately up to 0.145. The flow curves are obtained for two reasons. One reason is to use these flow curves in the macro rolling simulations and another to fit the material dependent parameters of the constitutive model discussed in Section 2.1. The experimental flow curves can be seen in Figure 1. The fitting procedure will be discussed in the following section.

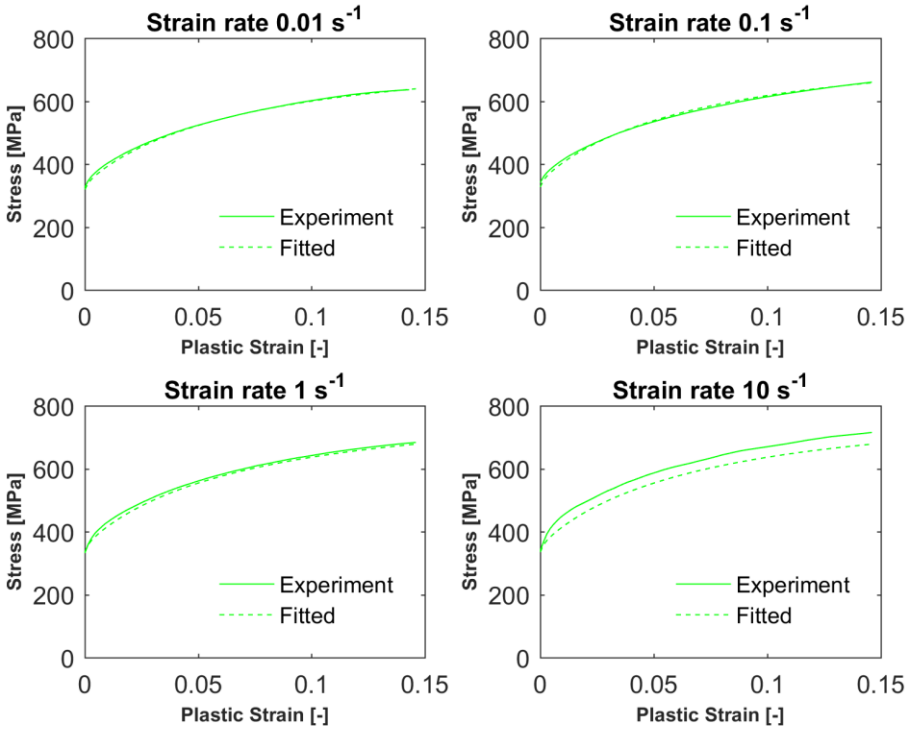

Figure 1: Experimental and fitted flow curves (Fitting procedure in Section 2.3).

2.3 Fitting Procedure

The parameter n in equation (2) influences the strain rate sensitivity of the constitutive model. It is observed in the stacked layer compression tests performed at room temperature, that silicon based steel considered in this work does not show much dependency on strain rates. Very high values of n (above 100) ensures the constitutive model strain independent, at the same time makes the model computationally expensive because the model is highly non-linear between the acting (resolved) stress and the resulting shear rate (governed by the magnitude of n). In this paper, using the flow curves obtained from compression tests, the strain rate sensitivity parameter is calculated with the following equation

$$n(\varepsilon, \dot{\varepsilon}) = \frac{\ln\left(\frac{\dot{\varepsilon}(\varepsilon)}{\dot{\varepsilon}(\varepsilon)^{ref}}\right)}{\ln\left(\frac{\sigma(\varepsilon, \dot{\varepsilon})}{\sigma(\varepsilon, \dot{\varepsilon}^{ref})}\right)} \tag{4}$$

where $\dot{\varepsilon}^{ref}$ is the reference strain rate. In this case the lowest strain rate from the experiments,

0.01 s^{-1} is used as reference. The mean value of individual flow curve is calculated and the average of the three flow curves is considered as the overall strain rate sensitivity. The mean value of the strain rate sensitivity is plotted in Figure 2.

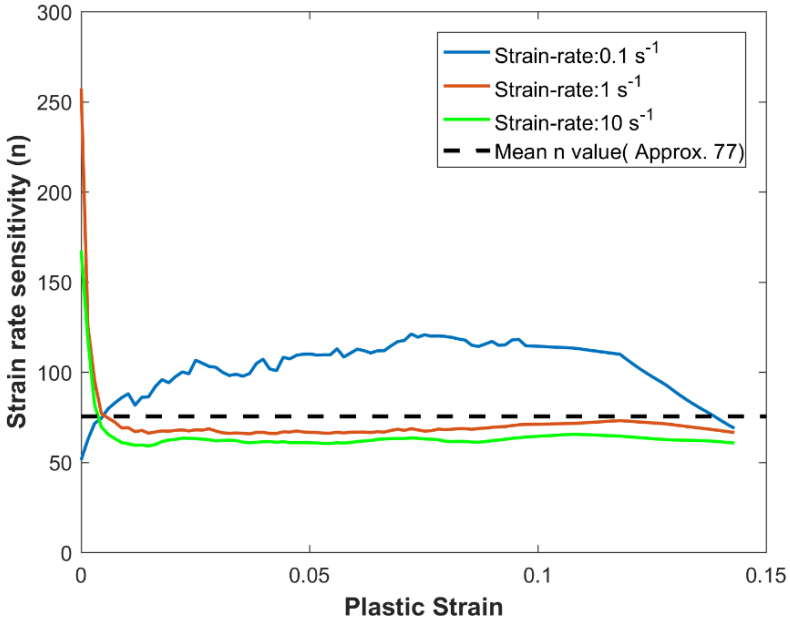

Figure 2: Strain rate sensitivity parameter calculation.

The other material dependent parameters were fitted by applying a compression displacement on an RVE at strain rate of 0.01 s^{-1} in the DAMASK spectral solver. A spectral solver is used for optimization of the parameters considering the computational costs. A 2D RVE with 300 grains was modelled for the spectral solver and a compression displacement was applied along the normal direction (ND). Initially a simulation was performed with some randomly selected material parameters. An objective function as a least square fit between the experimental and simulation results was formulated with the extracted flow curve and the experimental data. The objective function is shown in equation 5.

$$f = \sum_{k=0}^{m} \sqrt{((\sigma^{exp}(\varepsilon_k) - \sigma^{sim}(\varepsilon_k))^2} \tag{5}$$

where σ^{exp} and σ^{sim} are the experimental and simulation flow stress at strain ε_k, respectively.

A best fit for the material data is obtained by an optimization loop using the *fmincon* function in MATLAB. The tolerance limit is set to 1e-06 and maximum of 1000 iterations is allowed. The optimization algorithm is described in Figure 3. The fitted parameters are shown in Table 2 and the fitted flow curves along with the experimental flow curves are plotted in Figure 1. C_{11}, C_{22}, C_{44} are the elastic constants adapted from literature [8].

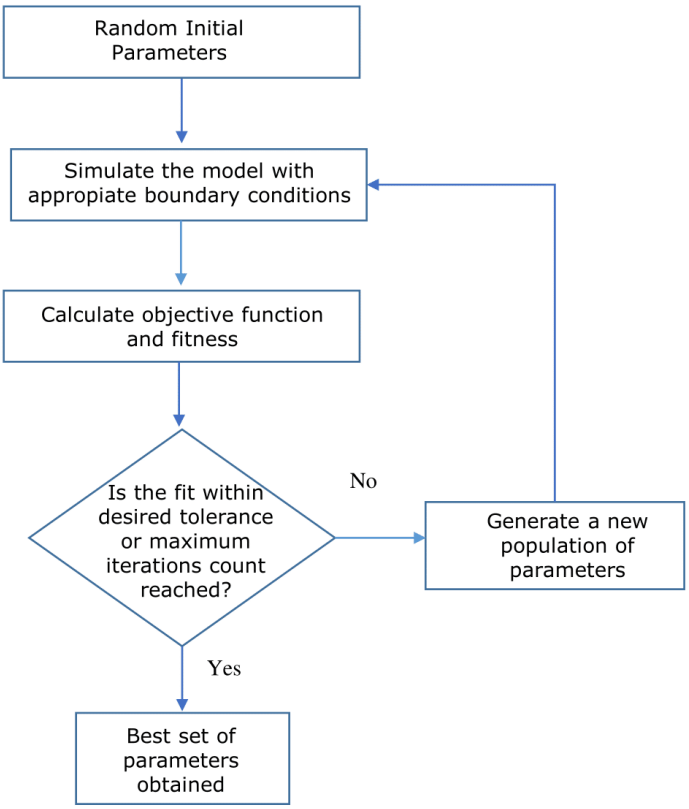

Figure 3: Optimization algorithm used in the flow curve fitting procedure.

Table 2: Parameters used for the phenomenological CPFEM model

Elastic parameters [8]						
$\mathbf{C_{11}}$		$\mathbf{C_{12}}$		$\mathbf{C_{44}}$		
232.2 GPa		135.6 GPa		117.0 GPa		
Plastic parameters						
	$\dot{\gamma}_0$	**n**	τ_0^c	τ_∞	$\mathbf{h_0}$	**a**
<111>{110}	0.01 s^{-1}	77	174.54 GPa	315.45 GPa	2.65e+09	2.11
<111>{211}	0.01s^{-1}	77	143.23 GPa	344.60 GPa	2.65e+09	2.11

2.4 Simulation Setup

2.4.1 Macro Simulation

A three pass rolling process is simulated in ABAQUS/Standard with appropriate boundary conditions and symmetries. The coordinate history of nodes in the center of the workpiece is extracted from the simulation to obtain the deformation gradient. The macro model is described in more detail in our previous work [7].

2.4.2 Micro Simulation

An 3D RVE with 300 grains is used in this paper. The RVE is modelled and meshed with 17576 hexagonal elements using the polycrystal generator software NEPER [9]. The 300 grains in the RVE have a grain size that is statically equivalent to the measured grain size in the experiments. At first, an Orientation Distribution Function (ODF) is calculated from the orientations extracted from XRD measurements using MTEX [10]. Then 300 orientations were selected from the calculated ODF using the discrete sample function in MTEX. The kernel halfwidth used for the discrete orientations is obtained from the default MTEX functions that calculate the optimal halfwidth. The RVE is shown in Figure 4 (a). Deformation gradient obtained from the macro simulation is imposed on the RVE along with periodic boundary conditions (PBC). The opposite faces in the RVE are coupled with the macroscopic deformation gradient $\boldsymbol{F^M}$ as

$$\boldsymbol{u}_a - \boldsymbol{u}_b = (\boldsymbol{X}_a - \boldsymbol{X}_b)(\boldsymbol{F^M} - \boldsymbol{I}) \tag{6}$$

where $\boldsymbol{X_a}, \boldsymbol{X_b}$ are the position vectors of the opposite node pairs in the RVE undeformed configuration and $\boldsymbol{u}_a, \boldsymbol{u}_b$ are the history of the displacement vectors. The deformation gradient converted to the displacement gradient ($\boldsymbol{H = F^M - I}$) is applied on the auxiliary nodes, which in turn are connected to the nodes on the faces of the RVE. Displacement gradient ($\boldsymbol{H}$) used in this work is shown in Figure 4 (b). The 3D RVE is simulated with the material model discussed in Section 2.1. The material model is fitted for the flow curves up to 0.145 strain and is capable to extrapolate for higher strains.

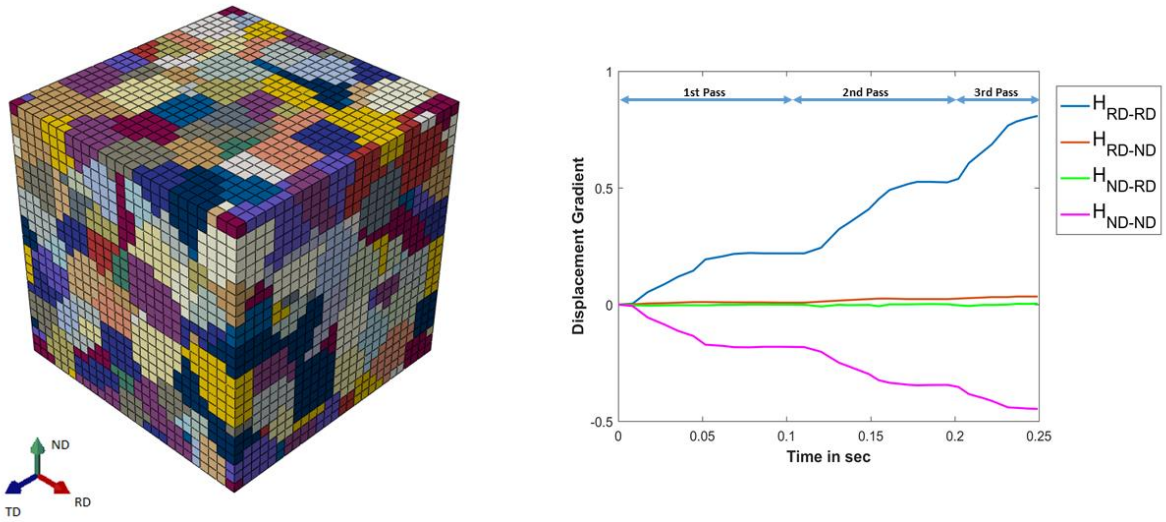

Figure 4: (a) RVE with 300 grains used for texture prediction (each color in the RVE represents a grain), **(b)** Displacement gradient applied on the RVE.

3 RESULTS

Figure 5 shows the results of the RVE deformation and the texture changes in the deformation process. Only φ_2=45° section of the full Euler space is shown, as it contains most of the important fibers (α-fibre, γ-fibre) needed in the study. Figure 5 (b) shows the results of the macro texture as intensity of orientation distribution function in the Euler space (φ_1, Φ, φ_2). The initial texture in Figure 5 (b) has most common orientations (0°, 15°, 45°) and (0°, 40°, 45°) like in the experimental measurements (Figure 5 (c)) and is assumed as a good

approximation of the initial texture. During rolling, the gradual increasing intensity of the α-fiber is well captured. In the simulation results, thought the orientations at (90°, 0°, 45°) are not observed before rolling, they could be well reproduced after the third pass.

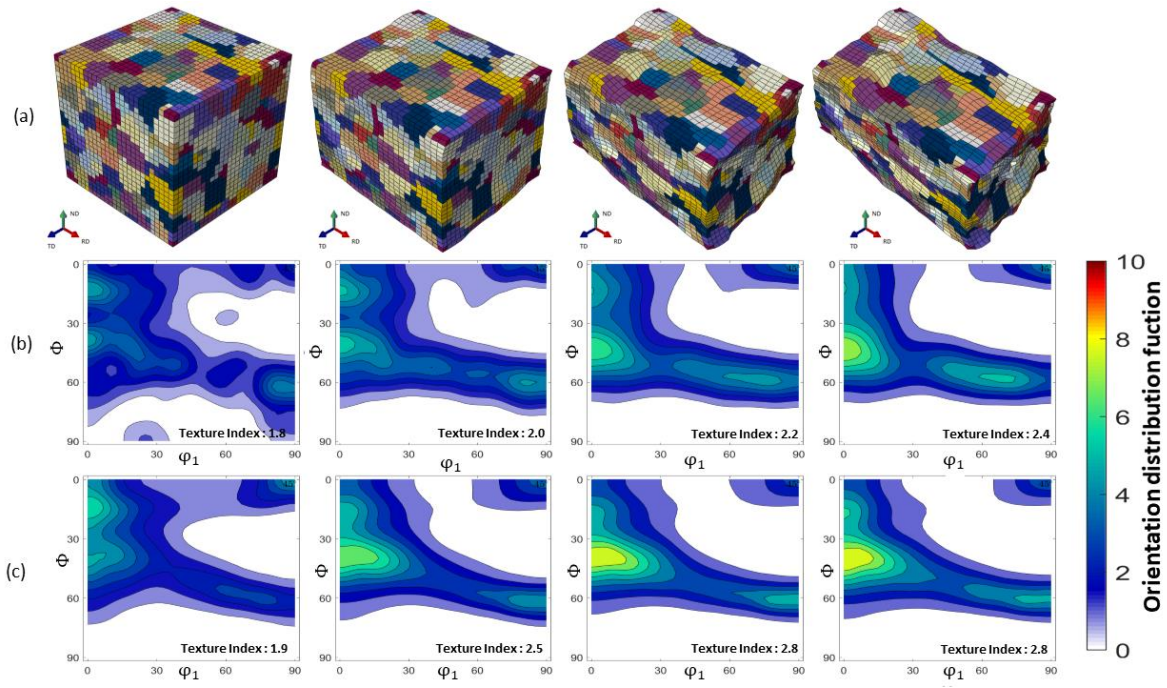

Figure 5: (a) RVE deformation under the applied boundary conditions for three passes (each color in the RVE represents a grain), **(b)** Simulation results for texture evolution during the rolling process for 50 % thickness reduction, **(c)** Experiment results for texture evolution during the rolling process for 50 % thickness reduction (Experiments conducted by IMM, RWTH Aachen). (Note: Figures (b), (c) are the φ_2=45° sections of the Euler space).

The texture evolution in rolling was simulated with a 2D RVE in our previous work [7]. The two basic assumptions with 2D RVE are plane strain conditions and the dimensions of the RVE (2D). To validate the first assumption, the 3D RVE described previously is forced to behave in plane strain conditions by manipulating the boundary conditions. RD-ND planes in the 3D RVE are fixed in the TD. In other words, from Figure 6 (a), the planes ABFE and DCGH will remain undeformed in the TD and are planar during the simulation. All other planes in the RVE will deform under the applied displacement gradient with periodic boundary conditions. The deformed RVE under these conditions is shown in Figure 6 (b) and can be observed that faces on the RD-ND planes remain planar and undeformed in the TD. The ODF after the third pass is shown in Figure 6 (c), and it can be seen that it is similar to the ODF for the third pass shown in Figure 5 (b). Therefore, the first assumption of plane strain is valid and has no influence on the texture evolution.

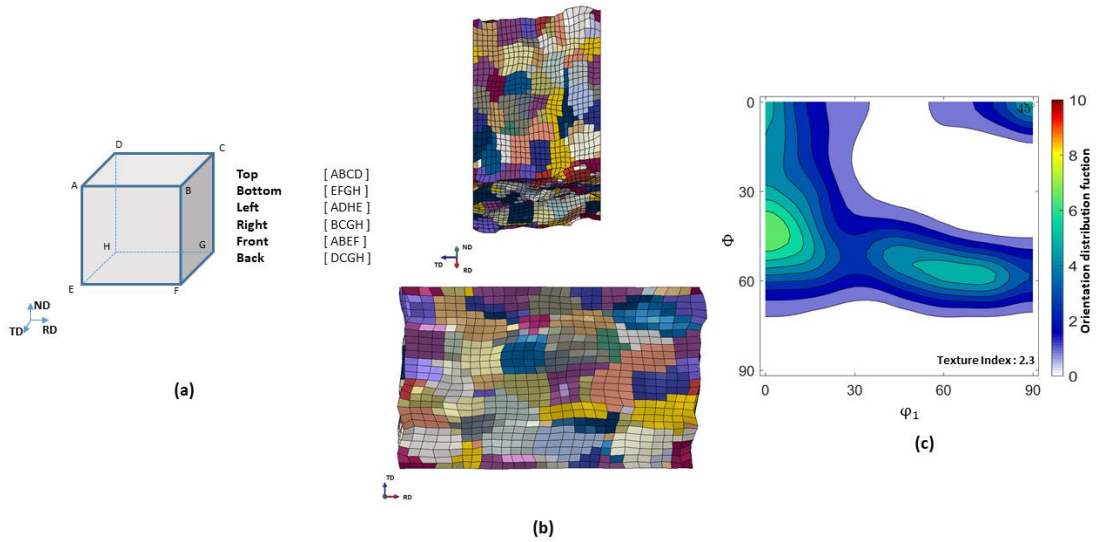

Figure 6: **(a)** RVE planar notation, **(b)** Deformed 3D RVE after third pass in plane strain condition (each color represents a grain), **(c)** ODF for plane strain 3D RVE after third pass.

The evolution of the fiber volumes of important texture fibers affecting the magnetic properties of electrical steels are shown in Figure 7. The figure shows the comparison of the fiber volumes for experiments, 3D RVE (unrestricted 3D and plane strain 3D) and 2D RVE presented in [7]. The considered 300 grains could not capture the initial fiber volume of α-fibre and ND cube fibres. This could be overcome by considering more grains inside the RVE. But the evolution of the experimental fibre volume could be well replicated in the 3D simulations. Similar to the experiments, the fiber volume of both α-fibre and γ-fibre increases in the 3D RVE simulations. The volume of ND cube fibre almost remains constant during the three pass rolling experiment and simulation. Moreover, the fibre volume of plane strain 3D RVE are similar to the unrestricted 3D RVE.

Though the 3D RVE considered in the study has approximately only 40-60 grains (compared to 300 grains in 2D) in the sections in the RD-ND plane, it could predict texture and fibre volume evolution more effectively compared to the 2D RVE. Thus it could be inferred from the discussed results that, a 3D RVE model is more efficient to predict the texture evolution in rolling simulations. Nevertheless, effects of different element types and grain interactions (for example misorientation) cannot be clearly separated based on the present results.

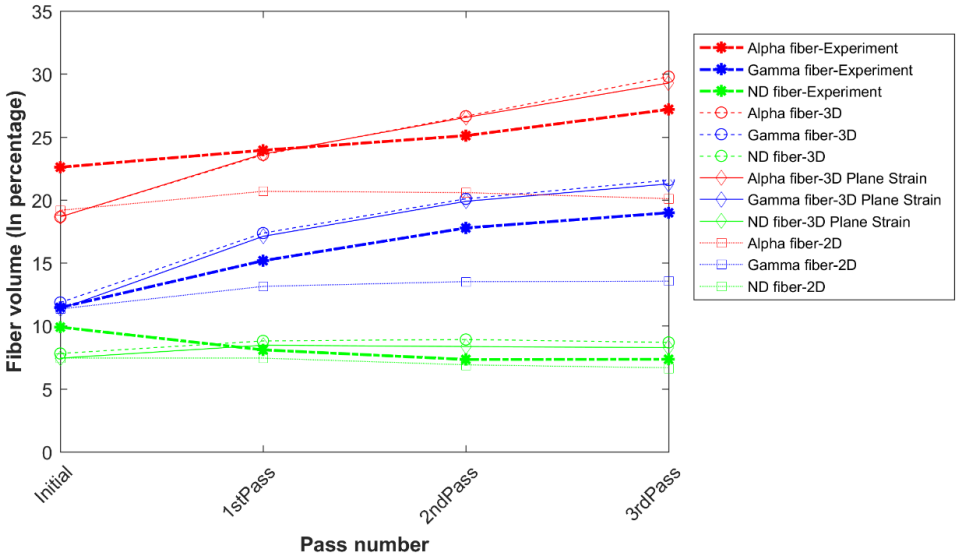

Figure 7: Comparison of fiber volume evolution during the three pass rolling for a 2D and 3D RVE.

4 CONCLUSION

In this paper, texture evolution in non-oriented silicon based electrical steels using a 3D RVE is studied. The phenomenological material model is fitted with upsetting tests simulated in the spectral solver environment in DAMASK. The boundary conditions are extracted from the macro simulation of a rolling process. The evolution of the typical α-fiber and γ-fiber could be replicated in the RVE simulation. It is observed that, 3D RVE could simulate the texture better than the 2D RVE especially for simulating rolling textures. Further research is needed to distinguish between the different possible influencing factors like the misorientation or the used element type. The currently developed model can be extended to simulate the texture at various locations along the strip thickness especially for the shear dominated regions near the surface. Also, the RVE morphology would be improved by incorporating the misorientation angle into the RVE from measured EBSD data.

5 ACKNOWLEDGMENTS

The authors would like to thank the Deutsche Forschungsgemeinschaft (DFG) for the financial support within the research group “FOR 1897- Low-Loss Electrical Steel Sheet for Energy-Efficient Electrical Drives”. The authors would also thank the Institute of Metal Forming (IMF) at TU Bergakademie Freiberg for providing the hot-rolled material and the Institute of Physical Metallurgy and Metal Physics (IMM) at RWTH Aachen University for their support within the XRD investigations.

REFERENCES

[1] Ghosh, P., Chromik, R. R., Knight, A. M., & Wakade, S. G. (2014). Effect of metallurgical factors on the bulk magnetic properties of non-oriented electrical steels. Journal of Magnetism and Magnetic Materials, 356, 42-51.

[2] Petrovic, D. S. (2010). Non-oriented electrical steel sheets. Materiali in tehnologije, 44(6),

317-325.

[3] Van Houtte, P., Li, S., Seefeldt, M., & Delannay, L. (2005). Deformation texture prediction: from the Taylor model to the advanced Lamel model. International Journal of Plasticity, 21(3), 589-624.

[4] Lebensohn, R. A., & Leffers, T. (1999). The rules for the lattice rotation accompanying slip as derived from a self-consistent model. Texture, Stress, and Microstructure, 31(4), 217-230.

[5] Roters, F., Eisenlohr, P., Hantcherli, L., Tjahjanto, D. D., Bieler, T. R., & Raabe, D. (2010). Overview of constitutive laws, kinematics, homogenization and multiscale methods in crystal plasticity finite-element modeling: Theory, experiments, applications. Acta Materialia, 58(4), 1152-1211.

[6] Eyckens, P., Xie, Q. G., Sidor, J. J., Delannay, L., Van Bael, A., Kestens, L. A., ... & Van Houtte, P. (2011). Validation of the texture-based ALAMEL and VPSC models by measured anisotropy of plastic yielding. In Materials Science Forum (Vol. 1517, No. 702, p. 233).

[7] Wei, X., Hojda, S., Dierdorf, J., Lohmar, J., & Hirt, G. (2017). Model for texture evolution in cold rolling of 2.4 wt.-% Si non-oriented electrical steel. In AIP Conference Proceedings (Vol. 1896, No. 1, p. 170005). AIP Publishing.

[8] Sha, X., & Cohen, R. E. (2006). First-principles thermoelasticity of bcc iron under pressure. Physical Review B, 74(21), 214111.

[9] Quey, R., Dawson, P. R., & Barbe, F. (2011). Large-scale 3D random polycrystals for the finite element method: Generation, meshing and remeshing. Computer Methods in Applied Mechanics and Engineering, 200(17-20), 1729-1745.

[10] Bachmann, F., Hielscher, R., & Schaeben, H. (2010). Texture analysis with MTEX–free and open source software toolbox. Solid State Phenom. 160, 63–68.